Numerical Optimization of 6D Cooling Solenoids for a Muon Collider

S. Fabbri, L. Bottura, and M. Statera

***Abstract*—In the current most evolved design concept of a machine for accelerating and colliding muons, there exists two long (∼1 km) channels for cooling newly created muons and anti-muons. Termed the '6D cooling channels', the beam is cooled in momentum and position space using a series of alternating polarity solenoids which create an oscillating field in the beam direction, absorbers and radio-frequency cavities. In total there are around 3000 solenoids per channel, contributing to a significant portion of the cost and engineering demands of the entire machine. The integration of the requirements of the field profile with feasible solenoid configurations is a difficult and unique problem, without analytic descriptions to readily relate these. We have addressed this problem in two ways: in the first we constrain the optimization studies of the optics by setting limits on solenoid parameters; in the second we have developed a numerical optimization routine to find the best configuration given a desired field profile, in terms of cost and engineering complexity. The following paper reviews semi-analytic descriptions of solenoids, select operating limits considering HTS, followed by the numerical optimization approach and subsequent results. This procedure is applicable to any solenoid or set of solenoids and can be an extremely useful optimization tool, running much quicker than current commercial softwares.**

***Index Terms*—Solenoid, accelerator magnets, muon collider, 6D cooling.**

I. Introduction

A MUON collider (MuC) holds tremendous potential as a next-generation tool for high-energy particle physics discoveries. Above ∼ 2 TeV, a MuC is expected to be the most energy-efficient choice for exploration of the energy frontier [1], and at 14 TeV, have a discovery potential similar to that of a 100 TeV proton collider [2]. While it is the muon properties (mass, point-like particle) which enable such superior effectiveness in a collider compared to protons or electrons, it's other property, a short lifetime at rest (2.2 μs), gives rise to significant and unique technical challenges.

In the present most advanced design concept of a MuC, a muon beam is generated by collision of a proton beam with a production target, resulting in a shower of pions which will decay into muons. These newly formed muons have a large spatial and energy spread, and thus must be cooled in six dimensions (6D) of the beam phase space (position and momentum) to reach values suitable for acceleration and high-luminosity collisions. This cooling process must occur before the muons decay completely. The only viable solution to achieve this is using ionisation cooling, which can be divided into two parts: 6D cooling and final transverse cooling. This paper discusses the former.

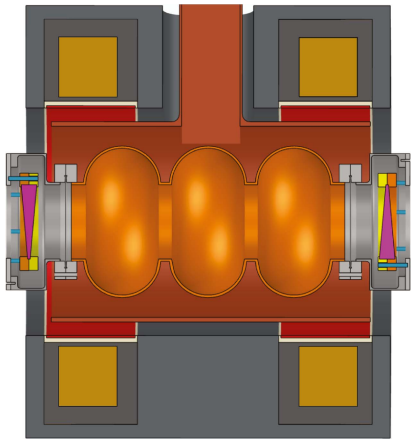

Fig. 1. A simplified conceptual design of an ionization cooling cell for a muon collider. Wedge shaped absorbers (pink) slow the beam in all directions, while RF cavities accelerate the beam longitudinally and alternating polarity solenoids confine the beam radially. CAD model by Mattia Castoldi.

In 6D ionization cooling, wedge-shaped absorbers and a dipole field reduce the beam energy in all directions and the longitudinal energy spread, RF cavities accelerate the beam longitudinally, and alternating polarity solenoids confine the beam radially. A simplified schematic of a 6D cooling cell is shown in Fig. 1.

The U.S. Muon Accelerator Program (MAP) study produced a baseline configuration of a 6D cooling channel, consisting of 826 cooling cells over an approximate 970 m distance, with a total of almost 3 k solenoids [3]. These cells can be divided into 12 unique types: A1-A4 and B1-B8. Each cell type contains between 2 to 6 solenoids, with a total of 18 unique solenoid types. For example, cell A1 has 4 solenoids, all of the same type, labeled A1-1, while cell B8 has 6 solenoids, of three different types, labeled B8-1, B8-2, and B8-3. The solenoids exhibit a diverse range of parameters, from small-bore to large-bore (90 mm to 1.5 m) and modest field to high field on-axis (2.6 T to 13.6 T). Each cell repeats a certain number of times (Ex. cell A1 repeats 66 times), before progressing to the next cell type. Fig. 2 displays

Received 25 September 2024; revised 27 November 2024; accepted 29 November 2024. Date of publication 10 January 2025; date of current version 30 January 2025. This work was supported by European Union (EU) under Grant 101094300. *(Corresponding authors: L. Bottura; M. Statera.)*

S. Fabbri and L. Bottura are with CERN, 1121 Geneva, Switzerland (e-mail: luca.bottura@cern.ch).

M. Statera is with INFN - LASA, 20090 Segrate, Italy (e-mail: marco.statera@mi.infn.it).

Color versions of one or more figures in this article are available at https://doi.org/10.1109/TASC.2025.3527957.

Digital Object Identifier 10.1109/TASC.2025.3527957

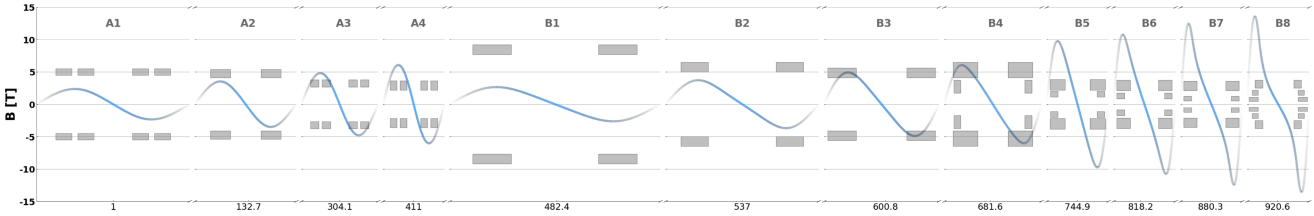

Fig. 2. Condensed schematic of the 12 types of cooling cells (A1 to B8) of a muon collider from the MAP configuration [3], with solenoid cross sections and the on-axis B_z field assuming each cell is in a lattice of neighboring cells of the same type. z-axis values shown correspond to the the middle of the first cell of each type.

TABLE I
TABLE OF VARIOUS PARAMETERS FOR 12 CELL TYPES AND 18 UNIQUE SOLENOID TYPES IN THE MAP CONFIGURATION

Cell	E_{Mag} (MJ)	e_{Mag} (MJ/m^3)	Coil	J_E (A/mm^2)	B_{peak} (T)	σ_{Hoop} (MPa)	σ_{Radial} (MPa)
A1	5.4	20.5	A1-1	63.25	4.1	34	–5/0
A2	15.3	75.8	A2-1	126.6	9.5	137	–28/0
A3	7.2	72.8	A3-1	165	9.4	138	–29/0
A4	8.4	91.5	A4-1	195	11.6	196	–49/0
B1	44.5	55.9	B1-1	69.8	6.9	95	–14/0
B2	24.1	61.8	B2-1	90	8.4	114	–20/0
B3	29.8	88.1	B3-1	123	11.2	173	–37/0
B4	24.1	42.4	B4-1	94	9.2	231	0/20
			B4-2	70.3	7.8	66	–24/0
B5	12	86.3	B5-1	157	13.9	336	0/21
			B5-2	168	12.3	159	–55/0
B6	8.2	68.3	B6-1	185	14.2	314	–1/22
			B6-2	155.1	10.3	118	–43/0
B7	5.6	58.6	B7-1	198	14.2	244	–1/21
			B7-2	155	10.1	118	–37/0
B8	1.4	20.3	B8-1	220	15.1	255	–3/22
			B8-2	135	6.2	110	–2/5
			B8-3	153	6.2	41	–23/0

Values correspond to solenoids operating in their respective cells within a lattice. Note that if the solenoid is operating standalone or in a single cell, some parameters take on higher or lower values.

the on-axis field of each cell type (assuming it is nested in a lattice of cells), and the solenoid cross-sections.

The solenoid configurations were designed to produce the required on-axis field profile, but otherwise were constrained in only two ways: the solenoid must fit in the free space not occupied by the RF cavities and beam pipe; the peak field in the solenoid does not exceed the limits of Nb $_3$ Sn [3]. We performed an analysis on these solenoids, considering them operating individually and within their respective lattice, using the commercial software COMSOL, reported in Table I. We found substantial stresses (large hoop and tensile radial stress), forces (37 MN axial force), and quench management challenges (energy densities up to 91 MJ/m^3 of a single coil). This motivated the development of a numerical optimization tool which can search ideal solenoid configurations given a desired field profile.

The International Muon Collider Collaboration (IMCC) is currently evolving the most advanced design concept of a MuC [4], [5]. Recently, a set of new optics has been developed in the 6D cooling channel which achieves an output transverse emittance that is half of what was achieved in previous studies [6]. This will aid in reaching a lower overall final emittance before acceleration and collision. During these beam dynamics studies, solenoid geometries and their corresponding field maps (among other parameters) are iterated on. To constrain the allowable magnet geometries and current densities, we provided a set of magnet 'design rules' in the form of a series of semi-analytic equations describing key solenoid parameters and corresponding allowed limits. This yielded a final optics with assumed solenoid geometries within or near allowed design limits.

The following paper reviews these key semi-analytic descriptions of solenoids and their corresponding imposed operating limits considering HTS, used in the latest design process. A newly developed numerical optimization tool is presented which can search large solutions spaces for ideal solenoids, with results shown for the MAP configuration.

II. SINGLE SOLENOID PROPERTIES

The following section considers a single solenoid revolved around the z-axis, as shown in Fig. 3. The magnetic field components arising from this solenoid can be described in 2D by B_z and B_r. Important parameters to describe the solenoid include the maximum field on-axis and peak field in the conductor, the self-stresses and forces, the stored magnetic energy, the self-inductance, and the critical current density J_c. These guide the design process when considering magnet engineering complexity, operation, and cost. The following sections give an overview of analytic and semi-analytic descriptions of some of these parameters, identification of their operating ranges, and visualization in the form of magnet aperture vs. magnetic field (A-B) plots.

A. Analytic and Semi-Analytic Descriptions

The field B_z along the z-axis of the solenoid in Fig. 3 with current density J can be derived analytically and written as,

$$B_z(z) = \frac{\mu_0 J}{2}\left[(z+L/2)\ln\left(\frac{\sqrt{R_f^2+(z+L/2)^2}+R_f}{\sqrt{R_i^2+(z+L/2))^2}+R_i}\right)\right.$$

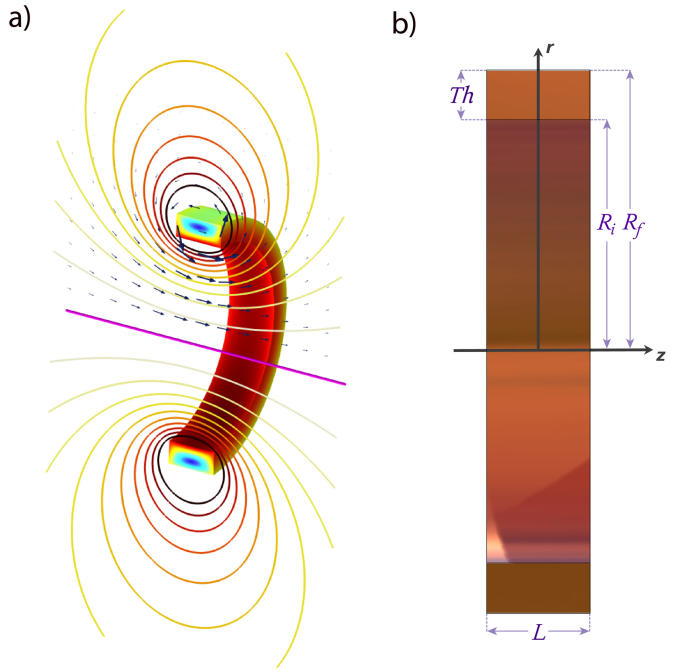

Fig. 3. Cross-section views of a single solenoid revolved around the z-axis, with magnetic characteristics shown in a) and key geometric parameters shown in b) such as the bore radius (R_i), thickness (Th), and length (L). In a) the magnetic field is visualized with contour lines of the normalized component and corresponding vectors indicating direction. The field intensity in the cross-section and surface of the coil is shown, with dark red indicating the highest field values and dark blue the lowest.

$$- (z - L/2) \ln \left(\frac{\sqrt{R_f^2 + (z - L/2)^2} + R_f}{\sqrt{R_i^2 + (z - L/2)^2} + R_i} \right) \Bigg]. \tag{1}$$

The peak central field on-axis $B_0 = B_z(0)$ is,

$$B_0 = \mu_0 J R_i \beta \ln \left[\frac{\alpha + \sqrt{\alpha^2 + \beta^2}}{1 + \sqrt{1 + \beta^2}} \right] \tag{2}$$

where $\alpha = R_f/R_i$ and $\beta = L/(2R_i)$.

The stresses, radial $\sigma_r(r)$ and hoop $\sigma_\theta(r)$, in the midplane ($z = 0$) of a solenoid subjected to a magnetic force density generated by the interaction of its self magnetic field with the current flowing through it can be approximated by solving a set of equilibrium equations with boundary conditions [7],

$$\sigma_r(\rho) = \frac{J B_1 R_i}{\alpha - 1} \left[\frac{2 + \nu}{3} (\alpha - \kappa) \left(\frac{\alpha^2 + \alpha + 1 - \alpha^2/\rho^2}{\alpha + 1} - \rho \right) \right. \tag{3}$$

$$\left. - \frac{3 + \nu}{8} (1 - \kappa) \left(\alpha^2 + 1 - \frac{\alpha^2}{\rho^2} - \rho^2 \right) \right]$$

$$\sigma_\theta(\rho) = \frac{J B_1 R_i}{\alpha - 1} \left\{ (\alpha - \kappa) \left[\frac{2 + \nu}{3} \left(\frac{\alpha^2 + \alpha + 1 + \alpha^2/\rho^2}{\alpha + 1} \right) \right. \right.$$

$$\left. - \frac{1 + 2\nu}{3} \rho \right]$$

$$\left. - (1 - \kappa) \left[\frac{3 + \nu}{8} \left(\alpha^2 + 1 + \frac{\alpha^2}{\rho^2} \right) - \frac{1 + 3\nu}{8} \rho^2 \right] \right\} \tag{4}$$

where $\rho = r/R_i$, ν is poisson's ratio of the material, B_1 and B_2 are the longitudinal field B_z at points $(r = R_i, z = 0)$ and $(r = R_f, z = 0)$ respectively, and $\kappa \equiv B_2/B_1$. The radial stress profile $\sigma_r(\rho)$ can take on both positive and negative values as a function of ρ, while the hoop stress profile $\sigma_\theta(\rho)$ will always be a positive value that decreases from its maximum at R_i to a minimum at R_f. A key assumption which enables the solutions $\sigma_r(\rho)$ and $\sigma_\theta(\rho)$ is that the $B_z(r, z)$ variation in the z-direction is insignificant, accurate for 'long' solenoids such as NMR magnets. The magnets focused on in this study are not 'long', and we observed errors up to ~ 10 % in the calculation of $\sigma_\theta(\rho)$. For $\sigma_r(\rho)$, the errors are small, except at small bore radii ($R_i \lesssim 100$ mm) where they can become large. With careful consideration and employing numerical methods where necessary, these equations can provide a quick approximation and are invaluable for scanning large geometry spaces.

Equations (3) and (4) rely on knowledge of B_1 and B_2. An accurate approximation of B_1 can be found using equations 3.12b and 3.15a in [7], however there is currently no mathematical expression for the field point B_2, but instead course estimations of κ (Ex. $\kappa = 0$ for an infinitely long solenoid). For solenoids in our geometry range, we found κ to vary from roughly -0.02 to -0.9. This wide variation in κ necessitates numerical methods to accurately estimate B_2.

The magnetic energy E_m of a solenoid can be calculated using the equation

$$E_m = \frac{1}{2} L I^2 \tag{5}$$

where L is the self inductance and I is the current in the conductor. There exist many equations for approximating the self inductance and mutual inductance of solenoids of different geometry, summarized in ref. [8]. Equation 86 in [8] is found to be the most accurate for our range of solenoid geometries, although it can have errors observed up to $\sim 5\%$ when the cross section of the solenoid is large relative to the mean radius. Using 86, the magnetic energy can be written as,

$$E_m = \frac{J^2 \mu_0 R_m (L \cdot Th)^2}{2} \cdot$$

$$\left(\ln \left(\frac{8 R_m}{\eta} \right) \left(1 + \frac{3\eta^2}{16 R_m^2} \right) - \left(2 + \frac{\eta^2}{16 R_m^2} \right) \right) \tag{6}$$

where R_m is the mean radius ($R_m = R_i + Th/2$) and η is a geometric factor $\eta = 0.2235(L + Th)$. Note that E_m is independent of knowledge of the conductor cross-section, because $L \propto N^2$ and $I \propto 1/N$ (where N is the number of conductor turns), N cancels. The magnetic energy density is the total magnetic energy divided by the volume of conductor,

$$e_m = E_m / V. \tag{7}$$

B. Operating Limits

The primary properties of a superconductor which can limit its performance are the critical current density (J_c) and the superconductor behavior under various mechanical load conditions, such as the mechanical stresses (σ_r, σ_θ and σ_z in a solenoid). To assess limits on these properties, we use HTS (ReBCO) from Fujikura FESC-SCH tape as a reference [9], which has a large dataset of J_c measurements [10] and stress measurements. The J_c measurements were used to fit an analytic description of the critical current density as a function of the operating temperature T_{op} and the field perpendicular to the tape plane (in a solenoid this is B_r) [11]. For analyses shown, we consider the following temperature and margin:

- HTS at $T_{op} = 20$ K and 2.5K margin

We consider a maximum average hoop stress (σ_θ) limit of 300 MPa [9], [12]. Although HTS has showed resilience at higher values, we take some margin to account for potential induced stresses during quench and stresses from edge-effects, magnetization and engineering uncertainties. For the radial stress (σ_r), we consider a maximum compressive stress of 300 MPa and a maximum tensile stress of 20 MPa [9]. The maximum tolerated tensile σ_r before degradation of the superconductor is approximately 10–100 MPa [13]. To avoid any tensile σ_r, a coil can be wound in tension generating a compressive pre-stress, such that there is no tensile σ_r when energized [14], making our initial tensile σ_r limit possibly conservative. Although we have no analytic description of the stress parallel to the axis of the solenoid (σ_z), we note that a compressive σ_z can be tolerated up to 100 MPa [9].

Lastly, the energy stored in these superconducting solenoids will be very large, and in the event of a quench (loss of superconductivity in the conductor), this energy will dissipate into heat. To prevent damage to the magnet during a quench from excessive temperature rise and induced stresses from non-uniform material expansion, limiting this stored magnetic energy is crucial. At this preliminary stage, a simplified estimation of the temperature rise during a quench can be computed assuming the magnetic energy is deposited homogeneously. Approximating the Fujikura FESC-SCH04 tape as 50 μm of Hastelloy C-276 and 60 μm of copper and using the specific heat capacity of these materials, with a magnetic energy density of 150 MJ/m^3 (16.8 kJ/kg), the temperature would increase to 128.3 K. This temperature rise could be reasonable, providing an initial acceptable upper limit. In the future detailed quench analysis studies will be necessary.

These parameter limits provide an initial framework for iterating the design study of all 6D cooling solenoids, while in parallel more detailed engineering analysis is being carried out for a proof-of-principle 6D cooling cell demonstrator with HTS solenoids.

C. A-B Plots

A useful visualization tool of the equations and their corresponding imposed limits described in the last two sections is a magnet aperture (A) vs. magnetic field (B) plot (A-B), where

TABLE II
LIMITS ON SELECT SINGLE SOLENOID PARAMETERS

Parameter	Unit	Lower bound	Upper bound
σ_θ	MPa	0	300
σ_r	MPa	–300	20
e_m	MJ/m^3	-	150

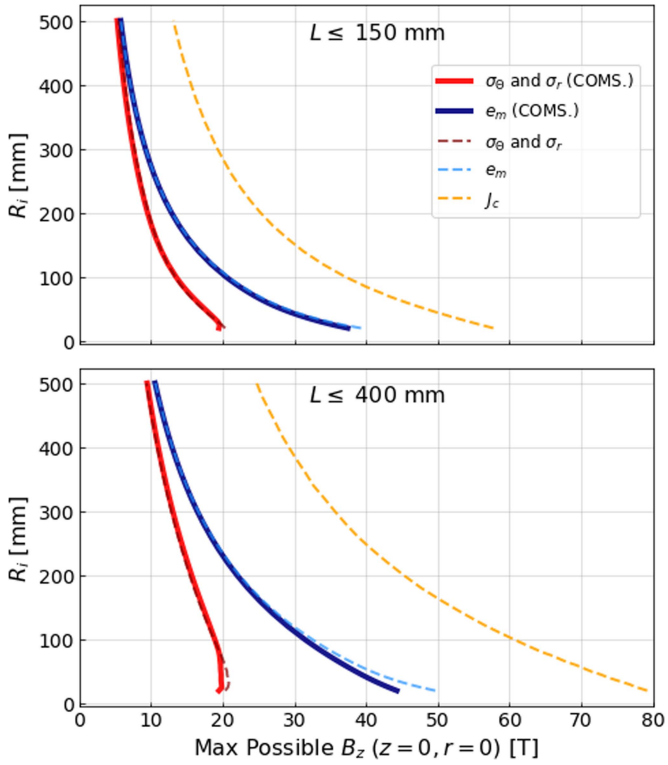

Fig. 4. The approximate maximum possible B_z on-axis versus bore radius (R_i) of a single solenoid with a maximum thickness of 340mm and a length up to 150mm (top) or 400mm (bottom), for different limiting parameters: red curves correspond to stress limits, blue to the magnetic energy density limit, and orange to the critical current density. Solid lines correspond to results found numerically with COMSOL (COMS.), and dashed lines to analytic or semi-analytic Eqs.

B is the maximum possible field on-axis (B_0 in (2)). Such plots have been part of the conceptual design process for the dipoles of the collider [15]. However, when considering solenoids there is added complexity because both the length and thickness of a solenoid can vary at a specified aperture. Both parameters must then be scanned over at a given bore radius, and different limits can be imposed depending on free space constraints.

The parameters focused on thus far to constrain the maximum allowable field **B** are the stresses σ_r and σ_θ ((3) and (4)), the magnetic energy density e_m (7), and the critical current density J_c, using limits described in Table II. Fig. 4 shows two example A-B plots for different limits of L. Results are shown using both numerical (solid curves) and semi-analytic (dashed curves) methods. As already discussed, numerical methods are required to provide field values as input for (3), (4) and J_c. Additionally, because (3) is not accurate at bore radii below $\sim$100 mm, these values can also be obtained numerically. Here, we used

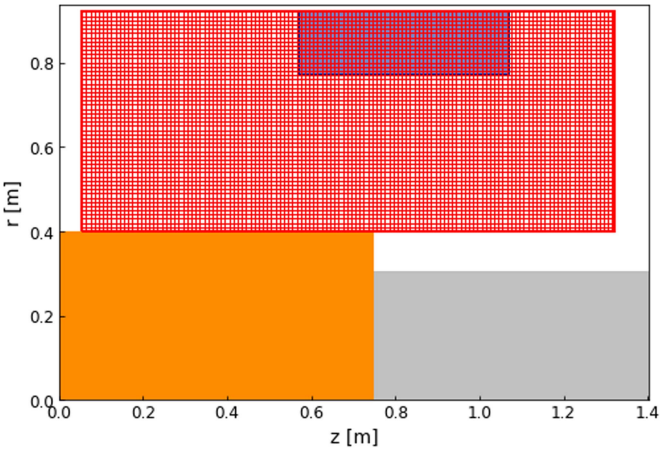

Fig. 5. Example of a mesh of current elements (red) generated for cell B1, where just half the cell is shown. The geometry of the original B1 coil by MAP is highlighted. Space required for RF cavities (orange) and the beam pipe (grey) with 50 mm for insulation are shown.

COMSOL to complete once a fine scan of single solenoids of varying dimension in the relevant geometry space ($(20 \leq Ri \leq 500, 50 \leq Th \leq 340, 80 \leq L \leq 400)$ [mm], ($\Delta Ri = 10$, $\Delta Th = 20$, $\Delta L = 20$) [mm]), providing a basis for accurate interpolation of these parameters.

Inspecting Fig. 4, in both L limits considered, up to $R_i = 500$ the stresses are the limiting constraint, while above this, e_m can become the limiting constraint. At bore radii below $\sim$100 mm the radial tensile stress can become the limiting constraint, while above this it is the hoop stress. At lower bore radii, (3) and (7) slightly overestimate the achievable B_0. Despite these inaccuracies, implementation of these equations in the form of a magnet design guide in the beam optics optimization process has been very successful.

III. Numerical Optimization Approach

The optimization of the solenoids for the 6D cooling channel is being carried out using a numerical code written in-house, termed the Solenoid in-Cell Optimization program (SiCO). This program is built to optimize solenoid configurations given a field profile corresponding to solenoids in a lattice, however it is also adapted to provide solutions corresponding to field profiles of single solenoids or single cells.

SiCO can be broken down into three steps, characterised by set-up, computation, and filtering based on the desired field profile and solenoid constraints. In the first step, the input is defined, including the desired on-axis field, the cell length L_C, the space a coil can exist within that cell (in z and in r), and the mesh size (Δz and Δr). The space constraints are set by the RF cavity dimensions and beam pipe dimensions, given in [3] and [6]. The RF cavity outer radius was calculated as $\approx 0.765\lambda/2$. An additional 50mm was added radially across the cell length to account for insulation and mechanical support of the coil. An example mesh of current elements is shown in Fig. 5.

Second, the program iterates through each current element, calculating its generated on-axis field B_z, assuming it is in a re-occurring lattice of alternating polarity elements. The on-axis field from 2 solenoids of opposite polarity and same geometry, placed within a cell of length L_C which is nested in an infinite re-occurring set of the same cells can be written using (1) as a infinite sum,

$$B_z^{\text{Lattice}}(z) = \sum_{i=0}^{\infty} \frac{\mu_0 J}{2} \left[(-1)^i B_z \left(z - \lceil \frac{i}{2} \rceil L_C + (-1)^i \frac{D}{2} \right) + (-1)^{i+1} B_z \left(z + \lceil \frac{i}{2} \rceil L_C - (-1)^i \frac{D}{2} \right) \right] \tag{8}$$

where $\lceil\ \rceil$ is the ceiling function and D is the distance between the solenoid centers. For each summation term, the field contribution of two solenoids is computed, with their central position shifted by $\mp(\lceil \frac{i}{2} \rceil L_C - (-1)^i (D/2))$.

Next, current elements are summed, both spatially and in their on-axis field contribution, to create larger cross-sections representative of solenoids. This is repeated for every unique rectangle within allowable size limits which can be created from the mesh. Because the number of unique rectangles which can be created from an NxM grid is $N(N+1)M(M+1)/4$, this is the most time-consuming step in the procedure.

Lastly, the solutions are filtered based on acceptable field error and single-solenoid parameter limits described in Table II. Because the solenoids are assumed in an infinite lattice, the field can be described as a harmonic series $B_z = \sum B_i \sin(2\pi z * i/L_C)$. The acceptable field error is provided by beam optics studies, and ranges in values of $2-3\%$ on each component of the first few harmonics of B_z. Each solutions's field (and current density) is scaled such that its maximum is equal to the maximum of the reference field, after which a fast Fourier transform is performed to obtain the harmonic components for comparison.

With this tool millions of solutions can be computed very quickly, allowing the choice of essentially the best solenoids depending on the design criteria. Additional considerations can be readily scanned, such as standardization (choosing solenoids across cells with the same geometry), powering and quench protection, etc. Calculation of the field only on-axis keeps the computation time low and enables the power of searching a wide solution space, however this also means the procedure misses two important considerations: the influence from neighboring solenoids (stress, peak field, etc.), particularly relevant to the radial stress profiles in 4-solenoid or 6-solenoid cells with solenoids at multiple radii; the homogeneity of the field off-axis in the beam region. Despite this, it provides an excellent starting point after which full-field computations can be used to fine-tune where needed.

A. Example - Cell B1

Cell B1 in the MAP design is characterised by two coils (coil type B1-1) each of length 500 mm, thickness 150 mm, bore radius 770 mm, and current density 69.8 A/mm^2 (alternating polarity), in a cell of length 2.75 m. It is the longest cell type, and has coils with the largest bore radius and coil volume of 0.398 m^3 per coil. This results in large stored magnetic energies,

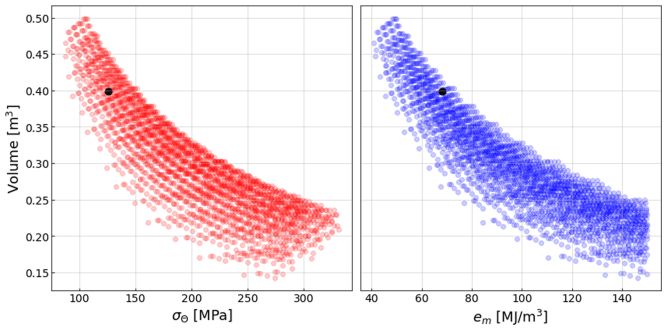

Fig. 6. Single solenoid volumes versus hoop stresses (left) and magnetic energy densities (right), corresponding to 2.4 k solutions which satisfy the input field of a B1 cell and parameter limits. The original B1-1 solenoid is shown in black.

with $e_m = 68$ MJ/m^3 in one coil. We can aim to significantly reduce the coil volume by considering HTS operating at a higher current density.

An example mesh of current elements for cell B1 is shown in Fig. 5. Because the cell is very large, we use a larger current element size of $\Delta z = 10$ mm and $\Delta r = 10$ mm to make the computation time required more manageable, as compared to 2.5 mm for smaller cells. The total number of current elements in the mesh shown is 127×53. Roughly 11.6 M unique rectangles can be built from this mesh, but with minimum and maximum length and thickness constraints imposed, 3.68 M unique rectangles are constructed. After filtering by acceptable error on each harmonic component, we are left with 74k solutions, and after further filtering based on acceptable parameter limits (σ, e_m, J_c), 2.4k solutions remain. The volume, hoop stress, and magnetic energy density of these final solutions are shown in Fig. 6. From a pure cost perspective, the coil volume could be reduced by 64%, corresponding to single solenoid parameters $\sigma_\theta = 235$ MPa and $e_m = 147$ MJ/m^3. If this solenoid is operated in a lattice, the stress in each solenoid reduces to $\sigma_\theta = 200$ MPa and 1 cell has $e_m = 126$ MJ/m^3.

IV. Present Results

We used the Solenoid in-Cell Optimization (SiCO) procedure discussed in the prior section to analyze cells A1 to B3 of MAP. Analysis of cells with coils at multiple radii (B4-B8) and new optics configurations [6] is ongoing and will be presented in the future. Optimization results presented here consider only 2 solenoids per cell. Fig. 7 presents the minimum achievable volume of conductor per cell for A1-B3, and the corresponding cell e_m and single coil stress σ_θ (values computed with COMSOL for solenoids in a lattice).

To achieve the minimum volume while maintaining the field profile, the current densities increase to values ranging from 160 A/mm^2 (B1-1) to 402A/mm^2 (A3-1). As expected, the hoop stresses and stored magnetic energies also increase (see Table I for comparison). However, other parameters stay similar or improve. The compressive radial stresses are low (maximum of 35.4MPa in coil A4-1, compared to 49MPa in MAP), with no tensile radial stress. The peak fields in the conductor are

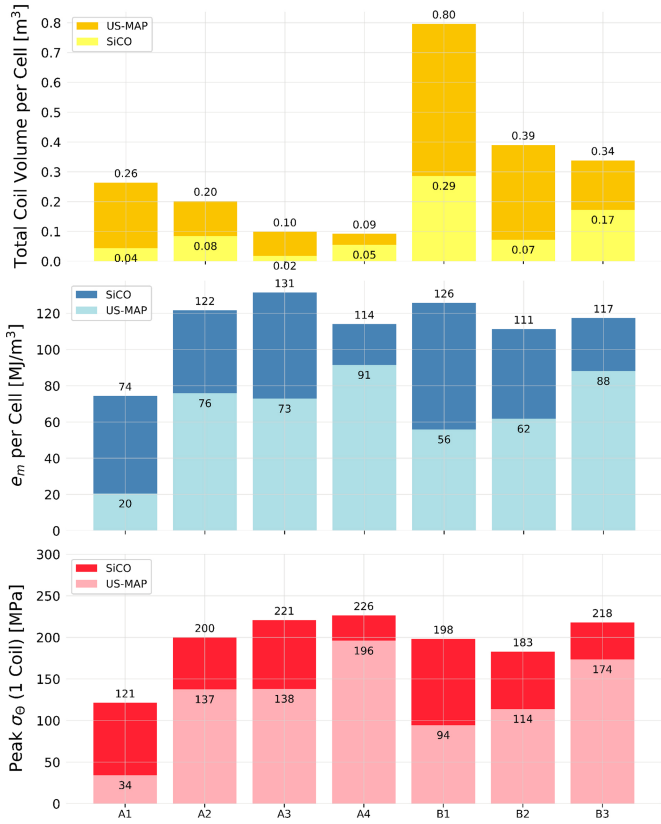

Fig. 7. Results of the minimum possible coil volume per cell (top) for cells A1 to B3, using the numerical optimization procedure (SiCO) compared to MAP values. The corresponding cell magnetic energy densities (middle) and peak average hoop stresses in each coil type (bottom) are shown, where values were computed with COMSOL for cells nested in lattices.

similar, with a maximum fraction of J_c reached in A3-1, with $J = 0.57 J_c$ ($B_{\text{peak}} = 8.2$ T). The net longitudinal forces are significantly smaller across all of the solenoids ($F_z = 36.8$ MN in MAP compared to $F_z = 12.4$ MN here for B3-1).

This solution set demonstrates the success of this numerical optimization tool to quickly search for the best solenoids depending on weighted design criteria and technology options. It provides an excellent starting point for more detailed mechanical analysis, where parameter limits can be easily changed to generate new solution spaces depending on evolving understandings. In the future results will be extended to include cells with more than 2 coils, and presented for updated optics such as those in [6]. These analyses are ongoing and aim to factor in more complex considerations such as standardization and powering.

V. Summary

This article has presented important analytic and semi-analytic descriptions of single solenoid parameters such as stresses and stored magnetic energy density, and their established acceptable limits suitable to guide the magnet design in a 6D cooling channel of a MuC. The described design process consists of two phases: in the first, this set of magnet 'design rules' constrains ongoing beam optics studies; in the second, a numerical tool has been developed to optimize existing [3] and

evolving magnet configurations [6]. We have demonstrated the power of this numerical optimization tool to search thousands of potential configurations so the best solenoids can be selected based on cost and magnet engineering complexity. The next step will be analysis of more complex cooling cells which require more than 2 solenoids, and further considerations such as standardization.

ACKNOWLEDGMENT

Views and opinions expressed are however those of the author(s) only and do not necessarily reflect those of the EU or European Research Executive Agency (REA). Neither the EU nor the REA can be held responsible for them.

REFERENCES

[1] K. R. Long, D. Lucchesi, M. A. Palmer, N. Pastrone, D. Schulte, and V. Shiltsev, "Muon colliders to expand frontiers of particle physics," *Nature Phys.*, vol. 17, no. 3, pp. 289–292, Jan. 2021, doi: 10.1038/s41567-020-01130-x.

[2] C. Aime et al., "Muon collider physics summary, 2022, *arXiv:2203.07256*.

[3] D. Stratakis and R. B. Palmer, "Rectilinear six-dimensional ionization cooling channel for a muon collider: A theoretical and numerical study," *Phys. Rev. Special Top.-Accelerators Beams*, vol. 18, no. 3, 2015, Art. no. 031003.

[4] L. Bottura et al., "Magnets for a muon collider–needs and plans," *IEEE Trans. Appl. Supercond.*, vol. 34, no. 5, Aug. 2024, Art. no. 4005708.

[5] S. Fabbri et al., "Magnets for a muon collider," in *J. Physics, Conf. Ser.*, vol. 2687, no. 8, 2024, Art. no. 082016.

[6] R. Zhu, C. Rogers, J. Yang, H. Zhao, C. Guo, and J. Li, "Performance and tolerance study of the rectilinear cooling channel for a muon collider," 2024, *arXiv:2409.02613*.

[7] Y. Iwasa, *Case Studies in Superconducting Magnets: Design and Operational Issues*. New York, NY, USA: Springer, 2009.

[8] E. B. Rosa and F. W. Grover, *Formulas and Tables for the Calculation of Mutual and Self-Inductance*, no. 169. Washingon, WA, USA: US Government Printing Office, 1948.

[9] Fujikura ReBCO HTS," Jul. 2024. [Online]. Available: https://www.fujikura.co.jp/eng/products/newbusiness/superconductors/01/superconductor.pdf

[10] S. Fujita et al., "Flux-pinning properties of $BaHfO_3$-doped EuBCO-coated conductors fabricated by hot-wall PLD," *IEEE Trans. Appl. Supercond.*, vol. 29, no. 5, Aug. 2019, Art. no. 8001505.

[11] B. Bordini et al., "Conceptual design of a ReBCO non/metal-insulated ultra-high field solenoid for the muon collider," *IEEE Trans. Appl. Supercond.*, vol. 34, no. 3, May 2024, Art. no. 4301310.

[12] H. W. Weijers et al., "High field magnets with HTS conductors," *IEEE Trans. Appl. Supercond.*, vol. 20, no. 3, pp. 576–582, Jun. 2010.

[13] H. Maeda and Y. Yanagisawa, "Recent developments in high-temperature superconducting magnet technology (review)," *IEEE Trans. Appl. Supercond.*, vol. 24, no. 3, Jun. 2014, Art. no. 4602412.

[14] H. Song, D. Hazelton, D. Fukushima, and P. Brownsey, "Engineering design and novel winding approaches in developing high quality HTS ReBCO coils," *IEEE Trans. Appl. Supercond.*, vol. 27, no. 4, Jun. 2017, Art. no. 4601305.

[15] D. Novelli et al., "Analytical evaluation of dipole performance limits for a muon collider," *IEEE Trans. Appl. Supercond.*, vol. 34, no. 5, Aug. 2024, Art. no. 4002405.